4198 *Biochemistry* **2009,** *48,* 4198–4208
DOI:10.1021/bi900009d

BIOCHEMISTRY
including biophysical chemistry & molecular biology
Article

The Toxicity of Prion Protein Fragment PrP(106−126) is Not Mediated by Membrane Permeabilization as Shown by a M112W Substitution†

Sónia Troeira Henriques,‡ Leonard Keith Pattenden,§ Marie-Isabel Aguilar,§ and Miguel A. R. B. Castanho*,‡

‡*Instituto de Medicina Molecular, Faculdade de Medicina da Universidade de Lisboa, Av. Egas Moniz, Edificio Egas Moniz, 1649-028 Lisboa, Portugal, and* §*Department of Biochemistry & Molecular Biology, Monash University, Victoria, 3800 Clayton, Australia*

Received July 18, 2008. Revised Manuscript Received February 27, 2009

ABSTRACT: Prion diseases result from a post-translational modification of the physiological prion protein (PrP^C) into a scrapie isoform (PrP^{Sc}). The PrP(106−126) fragment is conserved among various abnormal variants and shows PrP^{Sc} pathogenic properties. It has been proposed that the PrP(106−126) fragment may exhibit its toxic effects through membrane pore formation. Our previous studies showed that PrP(106−126) does not interact with membranes under physiological conditions. In the present study, PrP(106−126) affinity for membranes was increased by modifying PrP(106−126) with a M112W substitution, and pore formation was further evaluated. However, while the peptide exhibited an increased local concentration in the membrane, this did not lead to the induction of membrane permeabilization, as verified by fluorescence methodologies and surface plasmon resonance. These results further support the idea that PrP(106−126) toxicity is not a consequence of peptide−membrane interaction and pore formation.

Prion diseases, or transmissible spongiform encephalopathies, are characterized by neuronal accumulation of an anomalous scrapie isomer, PrP^{Sc} (*1*),[1] with physical properties profoundly different from the native PrP^C form; including greater β-sheet structure, resistance to proteolysis (*2*) and higher order aggregation into amyloid fibrils (*3*). Accumulation of PrP^{Sc} in the central nervous system is concomitant with progressive neuronal loss often accompanied by a spongiform encephalopathy. Once PrP^{Sc} is formed, it can accumulate in endosomes, in lysosomes, on the cell surface (*4*), or in extracellular spaces (*5*) in the form of amorphous deposits or amyloid plaques (*6*). The molecular details of this conformational transition of PrP^C into PrP^{Sc} are not clearly understood. Experimental evidence suggests that PrP^C is preferentially located in the cell membrane or more specifically in raft domains due to its glycosylphosphatidylinositol (GPI) anchor (*7*). The membrane surface is therefore likely to play a role in the conversion of PrP^C into PrP^{Sc}, and interaction of PrP with lipid membranes at the plasma membrane or in the endosomal/lysosomal pathway may be critical in the mechanism of prion toxicity.

The human PrP domain spanning amino acid residues 106−126 (KTNMKHMAGAAAAGAVVGGLG), PrP (106−126), is partially resistant to proteolysis, has neurotoxic activity, and has the capacity to readily form fibrils (*8*). Based on these observations, it was suggested that PrP (106−126) is a major contributor to the physicochemical and pathogenic properties of PrP^{Sc} (*9*). PrP(106−126) has therefore been proposed to play a role in conformational conversion of PrP^C to PrP^{Sc} (*10*) and is thought to be fundamental to the pathogenic mechanism common to different forms of prion disease (*11*). PrP(106−126) is therefore widely used as a model of PrP^{Sc}.

PrP(106−126) is characterized by an amphipathic primary structure with two domains: a hydrophilic N-terminal domain (KTNMKHM) and a hydrophobic C-terminal domain (AGAAAAGAVVGGLG). A propensity to interact with cell membranes was suggested (*12*)

†Fundação para a Ciência e Tecnologia (Portugal) is acknowledged for Grant SFRH/BD/14337/2003 to S.T.H. IUBMB is acknowledged for financial support to S.T.H. for a short-term visit to the MIA laboratory at Monash University, Victoria, Australia. The support of the Australian Research Council and the Potter Foundation is gratefully acknowledged.

*To whom correspondence should be addressed. E-mail: macastanho@fm.ul.pt. Phone: +351217985136. Fax +351217999477.

[1]Abbreviations: PrP, prion protein; GPI, glycosylphosphatidylinositol; HEPES, *N*-2-hydroxyethylpiperazine-*N*′-2-ethanesulfonic acid; POPC, 1-palmitoyl-2-oleoyl-*sn*-glycero-3-phosphocholine; POPG, 1-palmitoyl-2-oleoyl-*sn*-glycero-3-(phospho-*rac*-(1-glycerol)), *N*-NBD-PE, 1,2-dipalmitoyl-*sn*-glycero-3-phosphoethanolamine-*N*(7-nitro-2-1,3-benzoxadiazol-4-yl); *N*-Rh-PE, 1,2-dipalmitoyl-*sn*-glycero-3-phosphoethanolamine-*N*(lissamine rhodamine B sulfonyl); CHAPS, (3-[3-cholamidopropyl)-dimethyl-ammonio]-1-propanesulfonate; Chol, cholesterol; ANS, 1-anilinonaphthalene-8-sulfonic acid; di-8-ANEPPS, 4-(2-[6-(dioctylamino)-2-naphthalenyl]ethenyl)-1-(3-sulfopropyl)-pyridinium; CD, circular dichroism, REES; red-edge excitation shift; LUVs, large unilamellar vesicles; SUVs, small unilamellar vesicles; MLVs, multilamellar vesicles; SPR, surface plasmon resonance; DLS, dynamic light scattering; R_h, mean hydrodynamic radius.

 Published on Web 3/20/2009

and some studies ascribe PrP(106−126) neurotoxicity to peptide−lipid interactions, followed by pore formation events (*13*−*15*). Nevertheless, previous work in our laboratory revealed a low affinity of this domain for lipid membranes under physiological conditions (*16*). In order to increase the propensity of PrP(106−126) to interact with lipid membranes and further evaluate possible membrane pore formation, we undertook experiments with a tryptophan mutant, PrP(106−126)W, involving tryptophan substitution of an internal methionine (i.e., KTNMKHWAG AAAAGAVVGGLG). This tryptophan substitution is specifically localized between the hydrophobic and hydrophilic domains without disrupting the peptide amphipathicity or compromising the integrity of the core -AGAAA AGA- motif, which is important for overall peptide secondary structure and was implicated in modulating neurotoxicity (*10*,*17*).

Fluorescence data, together with surface plasmon resonance (SPR) analysis, allowed a detailed characterization of PrP(106−126)W−membrane interactions including calculation of the membrane partition coefficient, kinetics of peptide−lipid interaction, and assessment of the ability of PrP(106−126)W to form pores under different conditions including membrane charge, viscosity, pH, and ionic strength. PrP(106−126)W aggregation was also addressed by means of light scattering spectroscopy.

EXPERIMENTAL PROCEDURES

Materials. PrP(106−126)W (>95% purity) was purchased from Genscript (Piscataway, New Jersey). *N*-2-Hydroxyethylpiperazine-*N*′-2-ethanesulfonic acid (HEPES), sodium chloride, L-tryptophan, acrylamide, ethanol, and chloroform (spectroscopic grade) were obtained from Merck (Darmstadt, Germany). 1-Palmitoyl-2-oleoyl-*sn*-glycero-3-phosphocholine (POPC), 1-palmitoyl-2-oleoyl-*sn*-glycero-3-(phospho-*rac*-(1-glycerol)) (POPG), 1,2-dipalmitoyl-*sn*-glycero-3-phosphoethanolamine-*N* (7-nitro-2-1,3-benzoxadiazol-4-yl) (*N*-NBD-PE), and monoganglioside GM1 were from Avanti Polar Lipids (Alabaster, Alabama). (3-[3-Cholamidopropyl)-dimethyl-ammonio]-1-propanesulfonate (CHAPS) and cholesterol (chol) were obtained from Sigma-Aldrich (St. Louis, Missouri). 1-Anilinonaphthalene-8-sulfonic acid (ANS) and 4-(2-[6-(dioctylamino)-2-naphthalenyl] ethenyl)-1-(3-sulfopropyl)-pyridinium (di-8-ANEPPS) were obtained from Molecular Probes (Eugene, Oregon).

Working Conditions and Apparatus. UV−visible measurements were performed in a Jasco V-530 spectrophometer and fluorescence measurements were followed with a SPEX Jobin Yvon FluoroLog-3 spectrofluorometer equipped with 450 W Xe lamp and double monochromators. Fluorescence intensity values were corrected for inner filter effect when $A > 0.1$. SPR measurements were performed on a Biacore T100 (Biacore, GE Healthcare) with series S L1 sensor chips. Circular dichroism (CD) measurements were performed on a Jasco J-810 spectropolarimeter equipped with a temperature control unit. Dynamic light scattering (DLS) measurements were performed using a Malvern Nano ZS (Malvern, UK) apparatus with a constant 173° scattering angle.

PrP(106−126)W stock solution was prepared in sterile water (2 mg/mL; 1.05 mM). In the course of the experimental work, the peptide was studied and compared at cytoplasmic conditions (10 mM HEPES, pH 7.4, containing 150 mM NaCl (the so-called physiological ionic strength)) and also at acidic pH to mimic the endosomal medium (20 mM sodium acetate, pH 5, containing 150 mM NaCl). The effect of low ionic strength was evaluated at pH 5 (20 mM sodium acetate, 10 mM NaCl). Assays were performed at room temperature (25 °C).

Characterization of PrP(106−126)W in Aqueous Solution. The tryptophan fluorescence properties of PrP (106−126)W were used to obtain information on peptide behavior in solution. Spectral characterization, red-edge excitation shift (REES), and steady-state anisotropy studies were performed to examine the propensity for peptide aggregation at different pH. REES was followed by both fluorescence emission spectra shifts and variation of steady-state excitation fluorescence anisotropy in the range of 270−310 nm (methodological details have been published elsewhere, *18*).

Aqueous quenching of tryptophan fluorescence was followed using acrylamide with $\lambda_{excitation} = 290$ nm. Quenching assay data were corrected for the simultaneous absorption of light by fluorophore and quencher (*18*) and then analyzed using Stern−Volmer plots where

$$\frac{I_0}{I} = 1 + K_{SV}[Q] \quad (1)$$

(I and I_0 are the peptide fluorescence intensity in the presence and absence of quencher, respectively, K_{SV} is the Stern−Volmer constant, and [Q] is the quencher concentration).

The tendency of the peptide to aggregate was further evaluated by DLS at 25 ± 0.1 °C. PrP(106−126)W samples (50 μM) prepared in different buffer solutions were filtered through a sterile 0.22 μm Millipore filter (cellulose acetate). All the measurements were made at a fixed angle of 173° using an incident wavelength of 683 nm. For each sample, 15 scans were made with an individual collection time of 5 min. The autocorrelation scattering intensity data were processed with DTS software, version 5.10, to obtain the mean hydrodynamic ratio (R_h) of the particles by means of the cumulants method where the z-average of the diffusion coefficient (first cumulant) and variance (second cumulant) of the distribution are obtained (*19*).

Finally, changes in ANS fluorescence intensity were followed to detect nonpolar surface patches on the peptide (*20*). Briefly, ANS (12.8 μM) was titrated with a stock solution of PrP(106−126)W in the range 0−30 μM, and the fluorescence emission spectrum was recorded with excitation at 369 nm.

The effect of pH on the peptide organization state was also evaluated by means of ANS fluorescence. A sample containing 12.8 μM ANS and 25 μM PrP(106−126)W and a control without peptide were titrated with HCl, and the ANS fluorescence emission spectra were recorded at different pH.

Preparation of Lipid Vesicles for Peptide-Membrane Studies. Large unilamellar vesicles (LUVs) were used

throughout the study except for SPR studies where small unilamellar vesicles (SUVs) were used, and both vesicle types were prepared by the standard extrusion method. Briefly, lipids were dissolved in chloroform, and the solvent was removed under a N_2 stream to yield a lipid film, which was left to dry under vacuum overnight. The lipid film was hydrated with the desired buffer; upon agitation and eight freeze−thaw cycles, suspensions of multilamellar vesicles (MLVs) were obtained. The MLVs were extruded through polycarbonate filters (400 and 100 nm pore size, two and eight times, respectively) to obtain LUVs. For SPR measurements, vesicles were prepared by the same procedure but extruded with a 50 nm pore size (19 times) in order to obtain SUVs. SUVs were preferred for SPR experiments because they are less stable due to increased curvature strain of the liposomes and therefore they are easier to fuse and immobilize as a lipid bilayer onto the sensor chip surfaces.

Different lipid compositions were used throughout the studies: POPC and POPC/POPG (4:1 or 1:1 molar ratios) were prepared to test the effect of membrane charge at the liquid-crystalline phase. The possible effect of chol was evaluated in POPC/chol(2:1) vesicles. POPC/GM1 (9:1) membranes were used to test the possible effects of GM1.

PrP(106−126)W Partitioning into Lipid Membranes Based on Tryptophan Fluorescence. The fluorescence of tryptophan residues is highly sensitive to the local environment. A blue shift and an increase in quantum yield is detected when tryptophan is sequestered in a hydrophobic environment. The extent of partitioning of PrP(106−126)W into lipid membranes was investigated by the titration of PrP(106−126)W (25 μM) in solution with lipid suspensions (final lipid concentrations in the range 0−3 mM) and recording of the tryptophan emission fluorescence spectra following $\lambda_{excitation}$ = 278 nm. The peptide affinity for membranes was then quantified and compared among different lipid systems by the partition coefficient, K_P:

$$K_P = \frac{[\text{peptide}]_{\text{lipid}}}{[\text{peptide}]_{\text{aqueous}}} \quad (2)$$

which gives a relationship between the amount of peptide in solution and that interacting with the membrane (see ref *21* and references therein). If the peptide has a different quantum yield in the presence of lipid relative to the aqueous environment, the fluorescence intensity can be used to calculate the partitioning coefficient by nonlinear regression using eq 3 to fit I versus lipid concentration:

$$\frac{I}{I_W} = \frac{1 + K_p\gamma_L \frac{I_L}{I_W}[L]}{1 + K_p\gamma_L[L]} \quad (3)$$

(I_W and I_L are the total fluorescence emission intensities of the fluorophores when located in aqueous solution and in lipid solution, respectively; γ_L is the molar volume of lipid and is 7.63×10^{-1} dm^{-3} mol^{-1} for vesicles containing POPC, and [L] is the lipid concentration (*21*)). Assuming the peptide is restricted to the outer layer of the membrane since no translocation was detected for PrP(106−126) (*16*), data analysis was carried out taking into account the effective lipid concentration as being half of the total lipid concentration (*21*) except in Co^{2+}-quenching studies.

PrP(106−126)W Interaction with Lipid Membranes: SPR Methodologies. SPR is a sensitive technique for studying the interaction of peptides with lipid bilayers. This technique allows real-time monitoring of peptide binding to and dissociation from lipid bilayers and does not require peptide labeling. The interaction of PrP(106−126)W with lipid bilayers was further studied by SPR using liposomes composed of different lipid mixtures (1 mM lipid concentration; POPC, POPC/POPG (4:1), POPC/Chol (2:1), and POPC/GM1 (9:1)), which were deposited onto the L1 sensor chip surfaces (2 μL/min, 2400 s contact time). All solutions were freshly prepared and filtered (0.22 μm) before use. General SPR experimental details including lipid deposition and sensor chip surface regeneration followed methods described previously for PrP(106−126) (*16*), peptide injections PrP (106−126)W (0−30 μM) were injected over the lipid surfaces (20 μL/min, 180 s) and dissociation followed for 600 s per injection cycle. The sensorgrams for each lipid composition were analyzed by curve fitting using the BIAeval software (version 4.1). The data were fitted by applying the two-state reaction model. In this model, the first step is the initial peptide interaction with the membrane (the encounter complex) and is described by k_{a1} and k_{d1}. Peptide binding is followed by partitioning with reorientation or insertion of the peptide into the hydrophobic core (step two, described by k_{a2} and k_{d2}) (for further details, see ref *22* and references therein).

Secondary Structure Analysis by CD Spectroscopy. The secondary structure of PrP(106−126)W was studied using CD spectroscopy in the absence and presence of membranes. Samples containing 100 μM PrP(106−126)W with or without liposomes composed of POPC/POPG (4:1) (2 mM final lipid concentration; molar peptide/lipid ratio of 1:20) were prepared and measured at 25 °C in a quartz cell with an optical path of 0.1 cm. NaF was used in the buffer instead of NaCl to minimize buffer absorption. Spectra were recorded from 260 to 190 nm with a 0.1 nm step and 20 nm/min speed. Spectra were collected and averaged over five scans and corrected for background contribution.

Membrane Dipolar Potential Changes in the Presence of PrP(106−126)W. The membrane dipole potential, transmembrane potential difference, and the membrane surface potential are the three types of electrical potentials associated with membranes. The membrane dipole potential occurs at the membrane surface, and it seems to have its origin in the dipole moments of phospholipid headgroups and from water molecules in the transition region between the phases (*23*,*24*). These membrane dipoles can be affected by peptide insertion in the membranes (*25*). di-8-ANEPPS, located in the lipid headgroup region, is a dye sensitive to the local electric field of a membrane and therefore to the dipoles at the membrane surface. When the dipolar potential is altered, a spectral shift in the di-8-ANEPPS fluorescence excitation spectra is observed (*23*). This dye is not fluorescent in the aqueous medium, but when in the membrane, its fluorescence spectrum detects potential changes. PrP(106−126)W (25 μM) was added to LUVs with 200 μM lipid and

4 μM di-8-ANEPPS dye. Spectral variations in di-8-ANEPPS excitation were detected by subtraction of the spectrum ($\lambda_{emission}$ = 570 nm) in the absence of the peptide from the spectrum in the presence of 25 μM PrP (106−126)W (both spectra were normalized to total integrated area). The difference spectra reveal peptide-induced changes in the membrane dipolar potential. POPC and POPC/POPG (4:1 molar ratio) vesicles were used in these studies.

Membrane Leakage in the Presence of PrP(106−126)W. The ability of PrP(106−126)W to form pores was tested based on lipid-bound NBD fluorescence quenching by Co^{2+} ions (*16*,*26*). The permeability of the lipid bilayers to Co^{2+} ions in the presence of PrP (106−126)W was followed with vesicles (MLVs) doped with 1% of N-NBD-PE with 20 mM $CoCl_2$ outside the vesicles. Thus, initially Co^{2+} is accessible only to NBD present in the external layer. NBD fluorescence emission spectra were followed at $\lambda_{excitation}$ = 460 nm before and after PrP(106−126)W addition. POPC, POPC/POPG (4:1 molar ratio), POPC/POPG (1:1 molar ratio), and POPC/Chol (2:1) vesicles were used. Final lipid concentration of 100 μM and different PrP(106−126)W concentrations (0−50 μM) were left to incubate for 30 min and Co^{2+} was added to the samples afterward. For the positive control, lipid was hydrated with buffer containing 20 mM $CoCl_2$ to ensure that the quencher is accessible to the fluorophores in both the external and internal layers.

RESULTS

PrP(106−126)W Analogue Designed to Improve the Membrane Affinity. Interactions of proteins with membranes depend on specific properties of the membrane and amino acid side-chains such as charge, hydrophobicity, polarity, and capacity to establish H-bonding (*27*) and can be described mechanistically in different steps (*28*−*31*) involving initial attraction based largely on electrostatics (Coulombic and dipolar interactions and hydrogen bond formation, though hydrophobic interactions can play equally important roles), followed by hydrophobic partitioning, which can be transmembrane insertions or half-sided embedding, and finally membrane-induced conformational changes that can lead to a different membrane-dependent secondary structure or higher order assembly (e.g., pore formation).

We have previously shown that nonphysiological conditions (pH 5 and low ionic strength) increased the affinity of PrP(106−126) for membranes (*32*). However, the mechanistic steps involving the partitioning of the peptide from the bulk solution into the membrane interface is strongly dependent on the specific hydrophobic contribution of the individual amino acid residues (*28*,*33*), which based on White and Wimley analysis (*33*) (Figure 1) is very poor. In physiologically relevant ionic strength conditions, the interaction with the membrane was experimentally confirmed to be weak (*16*). Aromatic residues, such as tryptophan, have a particular affinity for the membrane interface (*27*,*33*) and are often present in protein transmembrane domains and in the case of tryptophan, the indole side chain is known to particularly

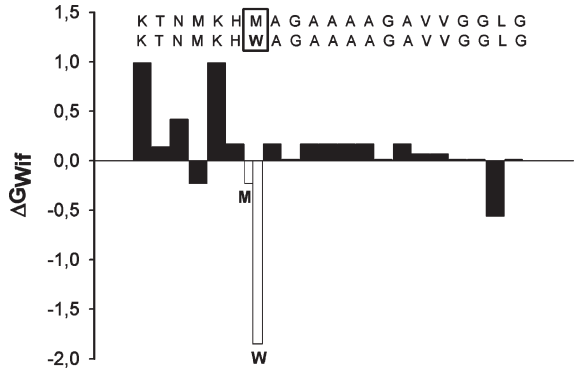

FIGURE 1: Theoretical analysis of PrP(106−126) and PrP (106−126)W tendency to partition to the interfacial membrane region. Prediction is based on the free energy change, ΔG_{wif}, for transfer from the water to lipid membrane interface. Residues with values $\Delta G_{wif} < 0$ have a tendency to be transferred from the water phase to the membrane interface. All the charged residues have highly unfavorable transfers, at variance with aromatic residues. The remaining residues make smaller contributions (*33*).

favor interactions with polar−apolar interfaces (*27*,*33*). PrP(106−126)W was designed to have an increased hydrophobicity and improved interfacial membrane partitioning properties as predicted by White and Wimley analysis (*33*) (see Figure 1).

PrP(106−126)W Aggregates in Aqueous Solution. Tryptophan fluorescence emission is sensitive to the microenvironment around the tryptophan residue. Therefore, the presence of a tryptophan residue in the peptide molecule provides a "hydrophobicity sensor". The fluorescence emission of a tryptophan residue exhibits a spectral maximum at about 350 nm when totally exposed to an aqueous environment (*18*), while a blue shift in the fluorescence emission spectrum indicates that the tryptophan residue is in a more hydrophobic environment. At pH 7.4 in the presence of 150 mM NaCl, PrP(106−126)W has an emission spectrum maximum at 343 nm; this blue shift indicates that the tryptophan is in a microenvironment not totally accessible to the aqueous environment and suggests that PrP(106−126)W is aggregated. The existence of REES (Figure 2A) indicates that there is a heterogeneous population of chromophores, which is also supportive of peptide aggregation. The quenching by acrylamide demonstrates that acrylamide is a less efficient quencher for PrP(106−126)W than for free L-tryptophan (K_{SV} = 9.5 ± 0.5 and 21.4 ± 0.5 M^{-1}, respectively), which confirms partial shielding of the tryptophan residue and further suggests peptide aggregation.

The effect of pH on peptide aggregation was evaluated by titration of PrP(106−126)W (25 μM, pH7.4, 150 mM NaCl) with 1 M HCl. The acidification effect on peptide fluorescence properties was compared with L-tryptophan as a control. At acidic pH, a decrease in quantum yield concomitant with a red shift in emission maximum was observed for the peptide (Figure 2B), while no significant effect was evident for L-tryptophan (data not shown). No REES effect was detected at pH 5 (data not shown). Nevertheless, the PrP(106−126)W quenching efficiency by acrylamide was not significantly modified at acidic pH (K_{SV} = 9.0 ± 0.2 M^{-1} in buffer containing 150 mM NaCl and K_{SV} = 8.6 ± 0.1 M^{-1} in buffer containing 10 mM NaCl).

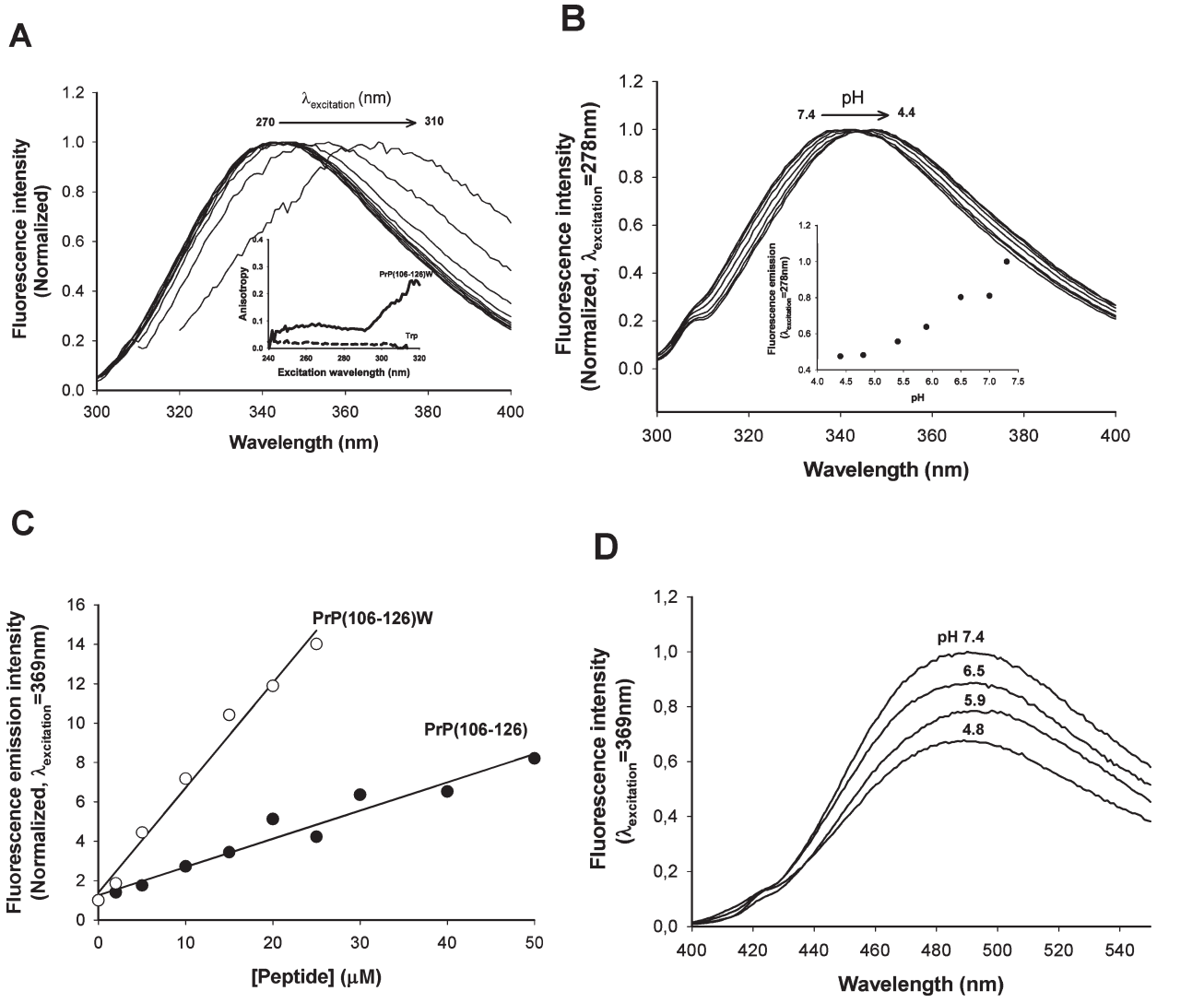

FIGURE 2: Characterization PrP(106−126)W in aqueous solution. (A) At pH 7.4, 150 mM NaCl, a red shift on PrP(106−126)W fluorescence emission spectra maximum (343−380 nm) occurs when excitation wavelength is increased in the range of 270−310 nm (REES). In the inset, an increase in fluorescence anisotropy with excitation wavelength confirms the REES effect; PrP(106−126)W (solid line) is compared with free tryptophan (dashes) in same conditions. (B) PrP(106−126)W fluorescence emission dependence on pH. Upon titration of 25 μM PrP(106−126)W with HCl, there is a red shift of emission spectra accompanied by a decrease on quantum yield (inset). (C) ANS fluorescence emission dependence on peptide concentration. ANS solution (12.8 μM) in HEPES, pH 7.4, containing 150 mM NaCl was titrated with PrP(106−126)W or with PrP (106−126). ANS fluorescence emission was followed with excitation at 369 nm. This effect is more pronounced for PrP(106−126)W than for PrP (106−126). (D) ANS fluorescence emission spectra ($\lambda_{excitation}$ = 369 nm) in the presence of 25 μM PrP(106−126)W upon titration with HCl (pH 7.4 and 150 mM NaCl is the initial condition).

PrP(106−126)W aggregation was confirmed by DLS measurements. With DLS, the fluctuation of the scattering light intensity on the microsecond time scale can be related to the diffusion coefficient of the scattering molecules. The diffusion coefficient obtained for the scatter is then converted in the size of a hard sphere with the same diffusion coefficient (*19*). Freshly dissolved PrP(106−126)W aggregates in all three buffers tested. DLS revealed that at pH 7.4 there is peptide aggregation ($\langle R_h \rangle$ = 70 nm with standard deviation = 9 nm), while for pH 5, this was not as pronounced: $\langle R_h \rangle$ = 21.4 ± 4.7 nm for pH 5, 150 mM, and 31.6 ± 1.6 nm for pH 5, 10 mM NaCl. These results confirm the ability of the PrP(106−126)W to aggregate in all the conditions tested and show that pH can influence the aggregation state of the sample.

To further examine the peptide organization/aggregation, experiments with ANS were undertaken as its fluorescence quantum yield is sensitive to the polarity of the environment and is frequently used to detect the presence of hydrophobic pockets in proteins and peptides (*20*). In agreement with the above tryptophan fluorescence results, an increase in ANS fluorescence intensity was observed along with a blue shift in fluorescence emission maximum upon PrP(106−126)W addition (Figure 2C), consistent with the existence of hydrophobic patches on peptide aggregates. Upon acidification, the ANS fluorescence in the presence of PrP(106−126)W was slightly decreased (Figure 2D). This suggests that the peptide organization is modified at acidic pH and further confirms DLS results where different scattering profiles were obtained when pH 7.4 or pH 5 were used. Overall, PrP(106−126)W is able to induce a larger increase in ANS intensity than PrP(106−126) (Figure 2C); this may arise from hydrophobic patches due to the presence of the tryptophan residue, which increases peptide hydrophobicity (Figure 1).

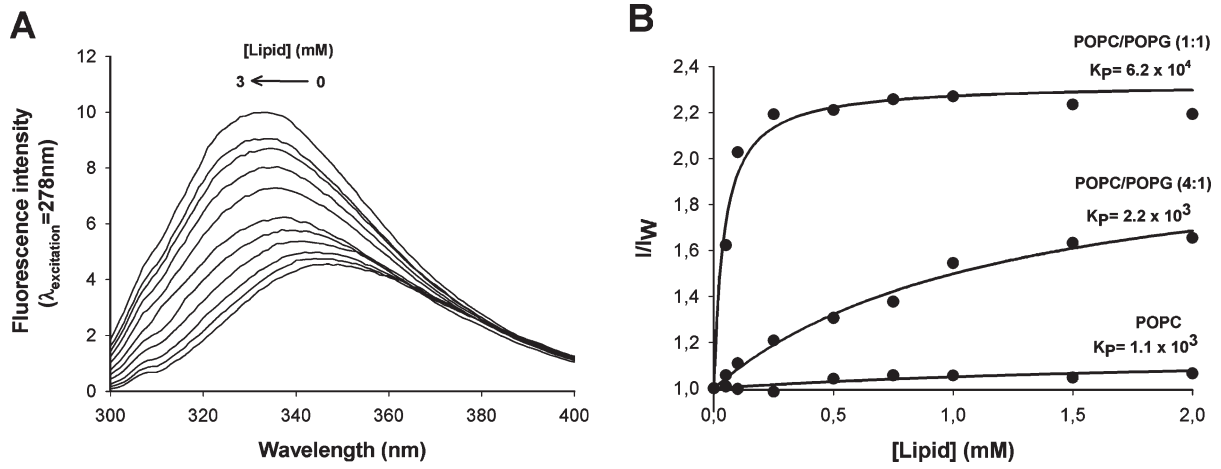

FIGURE 3: Membrane partitioning of PrP(106−126)W followed with 15 μM PrP(106−126)W in 20 mM acetate buffer, pH 5, containing 10 mM NaCl. (A) PrP(106−126)W fluorescence emission spectra ($\lambda_{excitation}$ = 278 nm) upon titration with POPC/POPG (4:1) LUVs. A blue shift, along with an increase in the quantum yield, suggests peptide insertion in the lipid bilayer. (B) Fluorescence emission of PrP(106−126) normalized to [lipid] = 0 (I/I_W) upon titration with LUVs of POPC, POPC/POPG (4:1), and POPC/POPG (1:1). Peptide affinity for different lipid compositions can be compared by means of K_P, obtained from nonlinear regression fitting (eq 3).

Hydrophobic and Electrostatic Interactions Contribute to PrP(106−126)W Partition into the Membrane. The interaction and affinity of PrP(106−126)W for lipid bilayers was studied either by fluorescence spectroscopy using large unilamellar vesicles (LUVs) or by SPR spectroscopy with suspended planar lipid bilayers formed on a biosensor surface.

At pH 7.4 with 150 mM NaCl, PrP(106−126)W has a $\lambda_{emission}$ maximum at 343 nm (Figure 2B). Titration of the peptide with lipid membrane resulted in no alterations in the tryptophan fluorescence emission spectrum. This can arise from the lack of interaction of the peptide with membranes or due to an insensitivity of the tryptophan to a more apolar environment if it is shielded within the peptide structure before lipid addition. A peptide can also have a high affinity for the membrane without exhibiting a large blue shift (*34*). As a consequence, peptide aggregation, arising from peptide−peptide interactions, may prevent modification of tryptophan fluorescence properties upon interaction with lipid.

At acidic pH, a blue shift and a quantum yield increase were detected in peptide fluorescence emission spectra upon titration with lipid suspension (Figure 3A, Table 1). The relationship between the amount of peptide in solution and that interacting with the membrane can thus be determined by the partitioning coefficient, K_P (eq 2). The influence of charge on the K_P values is also evident where they increased in the order POPC < POPC/POPG (4:1) < POPC/POPG (1:1) and were enhanced at low ionic strength (10 mM NaCl) (Figure 3B and Table 1).

The real-time monitoring of the peptide binding to and dissociation from lipid bilayer was followed by SPR, and the different conditions were further compared. Figure 4A shows a representative set of sensorgrams for the binding of PrP(106−126)W between 5 and 30 μM to immobilized POPC bilayers at pH 7.4 containing 150 mM NaCl and confirms that PrP(106−126)W is able to interact with phospholipid membranes at pH 7.4. These sensorgrams demonstrate a relatively slow association and low subsequent dissociation rates upon membrane binding (see Figure 4A and Table 2). These results

Table 1: PrP(106-126)W Partitioning into Lipid Membranes[a]

	pH 5, 150 mM NaCl		pH 5, 10 mM NaCl	
	K_P ($\times 10^3$)	blue shift (nm)[b]	K_P ($\times 10^3$)	blue shift (nm)
POPC		1	1.1 ± 0.5	6
POPC/POPG (4:1)	1.5 ± 0.9	2	2.2 ± 0.2	14
POPC/POPG (1:1)	9.3 ± 1.3	19	62 ± 5.8	20

[a] PrP(106−126)W samples (25 μM in 20 mM acetate buffer, pH 5, containing 10 mM NaCl or 150 mM NaCl) were titrated with LUVs and followed by tryptophan fluorescence emission ($\lambda_{excitation}$ = 278nm). [b] PrP(106−126)W fluorescence emission blue shift obtained upon addition of [lipid] = 3 mM.

are consistent with the peptide binding strongly via hydrophobic interactions and partitioning into the membrane.

The association of PrP(106−126)W with different membranes under the same buffer conditions shows very similarly shaped sensorgrams for all lipids (Figure 4B). The overall affinity values ranged from 1.26 × 10^6 M^{-1} for POPC/GM1 to 13.0 × 10^6 M^{-1} for POPC/POPG, revealing a slightly higher affinity for the anionic lipids and confirming that Chol did not contribute to the overall affinity (see Figure 4B and Table 2).

Similar results were obtained at pH 5 with high ionic strength (Table 2 and also Figure 4C) except the range of association constants K was between 1.56 × 10^6 M^{-1} for POPC/GM1 to 5.47 × 10^6 M^{-1} for POPC/POPG.

Figure 4C clearly shows that a decrease in ionic strength of the solution dramatically enhanced the association binding rates, even to the zwitterionic surfaces (Figure 4C). Specifically, the values for k_{a1} ranged from 13.2 × 10^2 to 24.4 × 10^2 M^{-1} s^{-1} (3.27 × 10^2 to 6.45 × 10^2 M^{-1} s^{-1} for high ionic strength). This is not surprising because a lower ionic strength increases electrostatic attractions between the peptide and the polar phospholipid headgroups and thereby increases the peptide concentration near the membrane (Figure 4C, D). Comparison of the affinity constants with different lipid surfaces and solution conditions reveals that PrP(106−126)

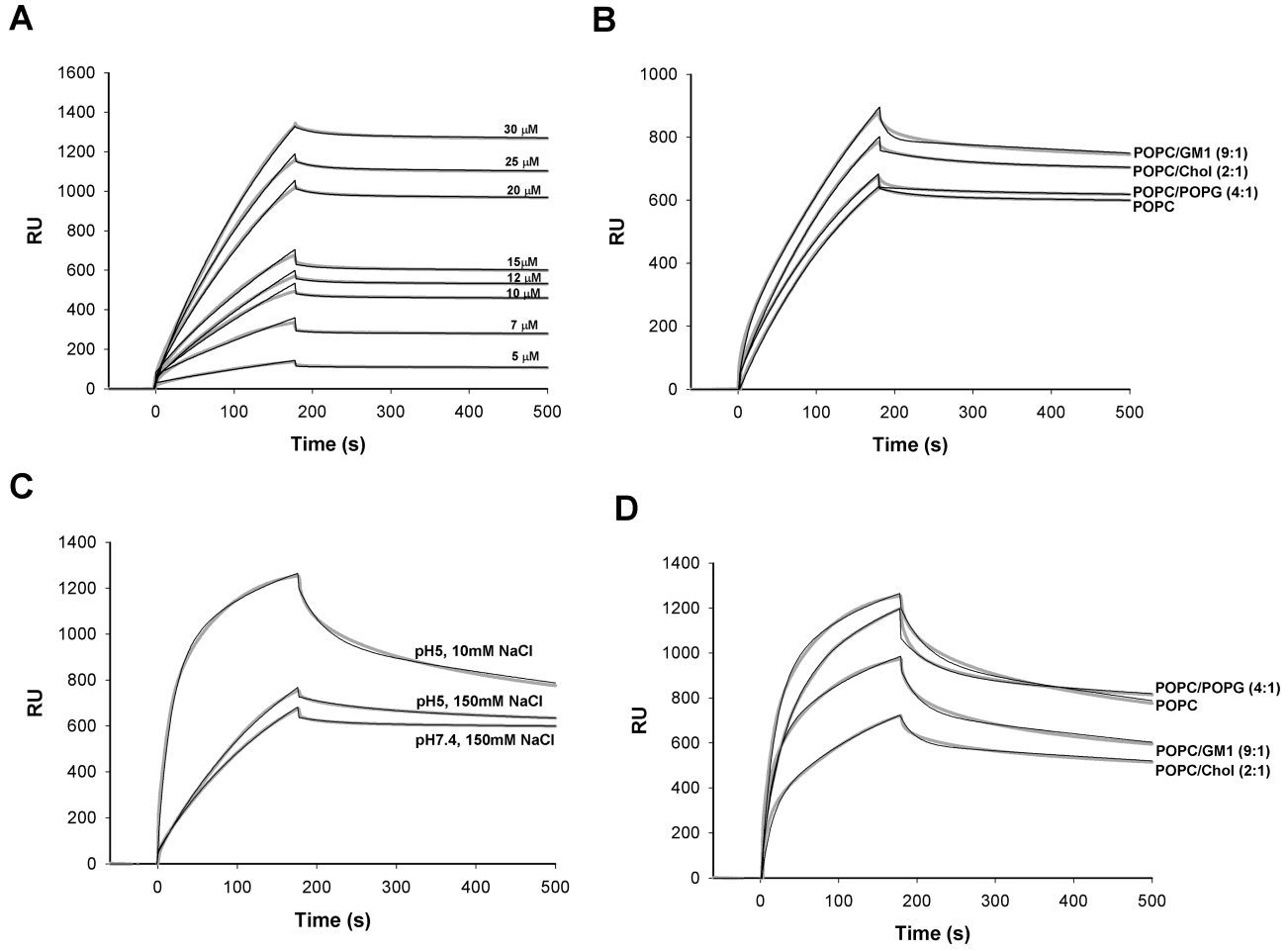

FIGURE 4: PrP(106−126)W membrane binding followed by SPR. Lipid surfaces were deposited on L1 chips. (A) Sensorgrams obtained for the binding of PrP(106−126)W between 5 and 30 μM to POPC membranes immobilized on the surface of L1 chip. Samples were prepared in HEPES buffer, pH 7.4, with 150 mM NaCl and injected over the surface with a flow rate of 20 μL/min. Sensorgrams were globally fitted with the two-state model (grey lines). (B) Sensorgrams for the binding of 15 μM PrP(106−126)W to membrane surfaces on L1 chips is shown for different lipid compositions at pH 7.4 and 150 mM NaCl. Compositions are POPC, POPC/POPG (4:1), POPC/Chol (2:1), and POPC/GM1 (9:1). Two-state binding model was fitted to data with BIAevaluation, version 4.1. Kinetic and affinity constants are presented in Table 2. (C) Buffer effect on 15 μM PrP(106−126)W affinity for POPC membranes. HEPES buffer, pH 7.4, with 150 mM NaCl, acetate buffer, pH 5, with 150 mM NaCl, and acetate buffer, pH 5, with 10 mM NaCl were used. (D) Sensorgrams for the binding of 15 μM PrP(106−126)W to membrane surfaces on L1 chips is shown for different lipid compositions at pH 5 and 10 mM NaCl: POPC, POPC/POPG (4:1), POPC/Chol (2:1), and POPC/GM1 (9:1). The two-state binding model was fitted to data with BIAevaluation, version 4.1. Kinetic and affinity constants are presented in Table 2.

Table 2: Association (k_{a1} and k_{a2}) and dissociation (k_{d1} and k_{d2}) rate constants, and affinity constant (K)[a]

	lipid type	$k_{a1} \pm$ SE ($\times 10^2$ M^{-1} s^{-1})	$k_{d1} \pm$ SE ($\times 10^{-3}$ s^{-1})	$k_{a2} \pm$ SE ($\times 10^{-3}$ s^{-1})	$k_{d2} \pm$ SE ($\times 10^{-4}$ s^{-1})	K ($\times 10^6$ M^{-1})	χ^2
pH 7.4, 150 mM NaCl	POPC	3.42 ± 0.02	4.14 ± 0.21	17.9 ± 0.4	2.75 ± 0.08	5.46	2
	POPC/POPG (4:1)	3.52 ± 0.03	0.40 ± 0.06	6.04 ± 0.89	4.39 ± 1.23	13.0	3
	POPC/Chol (2:1)	3.27 ± 0.04	1.72 ± 0.19	9.69 ± 0.71	3.04 ± 0.43	6.24	15
	POPC/GM1 (9:1)	6.45 ± 0.07	65.8 ± 1.1	31.9 ± 0.2	2.50 ± 0.02	1.26	37
pH 5, 150 mM NaCl	POPC	3.07 ± 0.04	2.43 ± 0.12	8.68 ± 0.32	7.09 ± 0.19	1.67	8
	POPC/POPG (4:1)	3.85 ± 0.04	3.94 ± 0.31	13.7 ± 0.4	2.94 ± 0.11	5.47	7
	POPC/Chol (2:1)	2.70 ± 0.04	2.22 ± 0.15	8.97 ± 0.42	5.81 ± 0.24	2.01	7
	POPC/GM1 (9:1)	4.42 ± 0.02	4.72 ± 0.06	8.85 ± 0.06	5.64 ± 0.38	1.56	6
pH 5, 10 mM NaCl	POPC	24.4 ± 0.3	20.5 ± 0.6	9.41 ± 0.10	9.00 ± 0.10	1.36	143
	POPC/POPG (4:1)	13.2 ± 0.7	12.4 ± 0.3	10.3 ± 0.1	5.07 ± 0.06	2.27	26
	POPC/Chol (2:1)	17.4 ± 0.3	41.3 ± 1.4	13.9 ± 0.2	5.47 ± 0.08	1.12	42
	POPC/GM1 (9:1)	22.7 ± 0.1	30.6 ± 0.3	10.9 ± 0.1	8.37 ± 0.04	1.04	110

[a] PrP(106-126)W (15 μM) binding to POPC, POPC/POPG (4:1), POPC/Chol (2:1), and POPC/GM1 (9:1) surfaces assayed in HEPES buffer, pH 7.4, containing 150 mM NaCl or in acetate buffer, pH 5, containing 150 mM NaCl or 10 mM NaCl. Lipid membranes were captured to L1 chip surfaces. Peptide samples were injected at 20 μL/min flow rate. Binding constants were obtained after fitting the SPR data to a two-state binding model with BIAevaluation version 4.1.

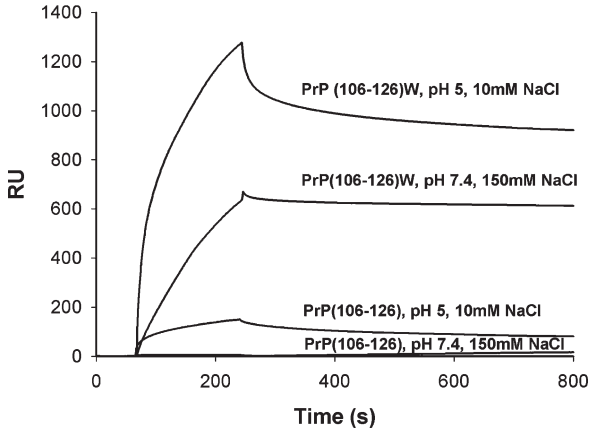

FIGURE 5: PrP(106−126) vs PrP(106−126)W binding to membranes followed by SPR. Comparison between 15 μM PrP(106−126) and 15 μM PrP(106−126)W binding to membranes composed of POPC/POPG (4:1) deposited over a L1 surface chip. Peptide was injected at a flow rate of 20 μL/min. Samples prepared in pH 7.4 buffer containing 150 mM NaCl were compared with samples prepared in pH 5 buffer containing 10 mM NaCl.

W has a greater affinity for the charged surface POPC/POPG than the neutral or Chol/GM1-containing surfaces (Table 2).

Altogether, results show that the peptide is able to interact with lipid membranes, even at pH 7.4, and confirms that hydrophobic forces are the determinants for the interaction of PrP(106−126)W with membranes and that electrostatic interaction increase the peptide association rate (see Figures 3 and 4 and Tables 1 and 2). Furthermore, a comparison of sensorgrams obtained with PrP(106−126) and with PrP(106−126)W on POPC/POPG (4:1) surfaces (Figure 5) show greater affinity of PrP(106−126)W compared with PrP(106−126), clearly highlighting the importance of the tryptophan residue to the increase in peptide−membrane affinities.

Secondary Structure: CD Spectroscopy. CD spectroscopy was used to evaluate peptide secondary structure changes upon interaction with lipid membranes. CD spectra obtained in the absence and presence of LUVs composed of POPC/POPG (4:1) are compared for the three buffers (Figure 6).

At pH 7.4 with 150 mM NaF, the minimum appears at 202 nm in the aqueous environment and no significant alteration occurs in the presence of lipids.

At pH 5, CD spectra have a minimum at 197 nm for both ionic strengths (150 mM NaF and 10 mM NaF). However, upon interaction with lipid membranes, a band shift to 204 nm occurs and a concomitant decrease in band intensity occurs in samples containing 150 mM NaF. At pH 5 and 10 mM NaF, the CD spectrum is significantly modified, which suggests a more significant conformational change in the presence of the lipid environment at low ionic strength. It could be argued that vesicle aggregation may have caused the spectral changes due to light scattering. However, turbidity measurements (not shown) revealed that there was no extensive vesicle aggregation in any of the conditions. Overall, the results are consistent with a decrease in the random coil content upon membrane interactions suggesting that PrP(106−126)W has a stronger membrane interaction at pH 5 at low ionic strength than in the other conditions tested.

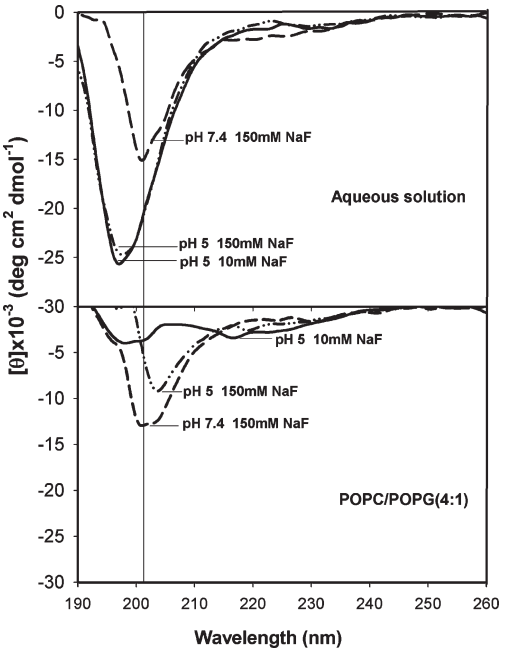

FIGURE 6: PrP(106−126)W CD spectra in presence and absence of lipid. Spectra were performed with 100 μM PrP(106−126)W in the absence and presence of POPC/POPG (4:1) LUVs ([lipid] = 2 mM). Three different buffers were tested: 10 mM HEPES buffer, pH 7.4, 150 mM NaF; 20 mM acetate buffer, pH 5, 150 mM NaF; 20 mM acetate buffer, pH 5, 10 mM NaF. At pH 7.4, both minima in the presence and in the absence of membranes remain at the same wavelength (202 nm). At pH 5 (both physiologic and low ionic strengths), the CD spectra have a strong negative band at 197 nm (random coil structure). Upon interaction with membranes a shift to 204 nm and a decrease in band intensity occurs at physiologic ionic strength. At low ionic strength, a significant alteration of spectrum profile with a decrease on band intensity is noted.

PrP(106−126)W Modifies Membrane Dipolar Potential but Does Not Form Ionic Channels. The presence of peptides in a lipid membrane can induce changes in dipole orientation and therefore in the membrane dipolar potential, and this perturbation can be studied using the fluorescence excitation spectra of the lipid probe di-8-ANEPPS. The blue spectral shift in fluorescence excitation spectra observed in the presence of PrP(106−126)W (Figure 7) indicates that the electronic structure of di-8-ANEPPS dye changes due to an increase in the membrane dipolar potential. This was found for all lipid systems tested, even at pH 7.4 with 150 mM NaCl, as shown in Figure 7, which is opposite to that observed with PrP(106−126). This result further confirms that PrP (106−126)W interacts with membranes.

The formation of large nonselective ion membrane channels induced by PrP(106−126) has been proposed as the cytotoxic mechanism of action of this prion peptide (*14*). However, our previous work shows that PrP(106−126) does not have significant affinity for the membrane, and therefore no membrane channel formation was detected (*16*). PrP(106−126)W has a greater affinity for lipid membranes than PrP(106−126), which could potentially result in membrane destabilization and permeabilization. The ability of PrP(106−126)W to induce membrane leakage was tested using the ability of Co^{2+} to quench NBD fluorescence. Different lipid mixtures were tested with the three buffers, but vesicle permeability did not occur at physiological ionic strength

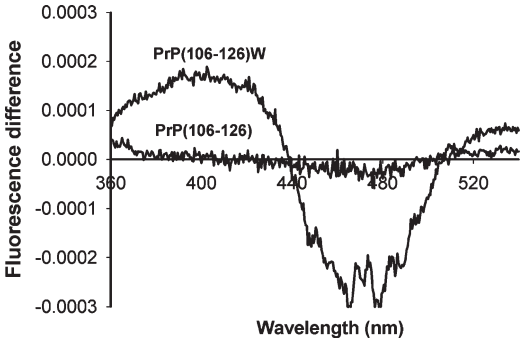

FIGURE 7: PrP(106−126) and PrP(106−126)W influence on the dipolar potential of lipid vesicles. Dipolar potential of POPC/POPG (4:1) LUVs ([lipid] = 200 μM) followed by fluorescence difference spectra of di-8-ANEPPS-labeled vesicles. Excitation spectrum obtained in the absence of peptide was subtracted from the spectrum obtained in the presence of 25 μM peptide in HEPES buffer, pH 7.4, containing 150 mM NaCl; both spectra were normalized to the integrated areas to reflect only the spectral shift. The difference spectrum obtained has a more pronounced shift for PrP (106−126)W than for PrP(106−126).

and is not significantly different from that obtained with PrP(106−126) (Figure 8A). Vesicle permeability was only noticeable at pH 5 at low ionic strength with POPC/POPG (1:1) membranes. Only under these extreme conditions is PrP(106−126)W able to cause the vesicles to leak. The addition of 5 μM PrP(106−126)W caused a leakage close to 100% (Figure 8B). The leakage efficiency is stronger than that verified with PrP(106−126) under these conditions (Figure 8B) (see also ref *16*).

Using K_P (Table 1), one can calculate the fraction of the peptide located in the lipid bilayers, X_L (see ref *18* for further details):

$$X_L = \frac{K_p \gamma_L [L]}{1 + K_p \gamma_L [L]} \quad (4)$$

The X_L obtained for 100 μM POPC, POPC/POPG (4:1), and POPC/POPG (1:1) at pH 5 and 10 mM NaCl is 0.08, 0.14, and 0.82, respectively. Hence, leakage occurs with POPC/POPG (1:1) because under these conditions the membrane is overloaded with peptide, which induces an extreme membrane stress (*35*).

DISCUSSION

The membrane binding of PrP^C via a GPI anchor and subsequent disease progression (*36*) and toxic effects of PrP(106−126) (*37*) suggest a strong interaction of this fragment with membrane lipid bilayers, with a specialized membrane components, such as GM1 or cholesterol. The effect on endogenous ion transport and ion channel formation and its toxic effects in neuronal cells have been studied (*13*,*14*,*38*−*40*), but while it has been hypothesized that neurotoxicity may occur due to pore formation, this hypothesis remains controversial (*41*,*42*).

Our previous work has shown that under more physiological conditions encountered in cytoplasmic or endosomal environments, PrP(106−126) has a low affinity for the membrane that is slightly increased both at low ionic strength and in the presence of negatively charged phospholipids but does not show any preference for membranes containing Chol or GM1, which excludes a specific interaction with these components (*16*).

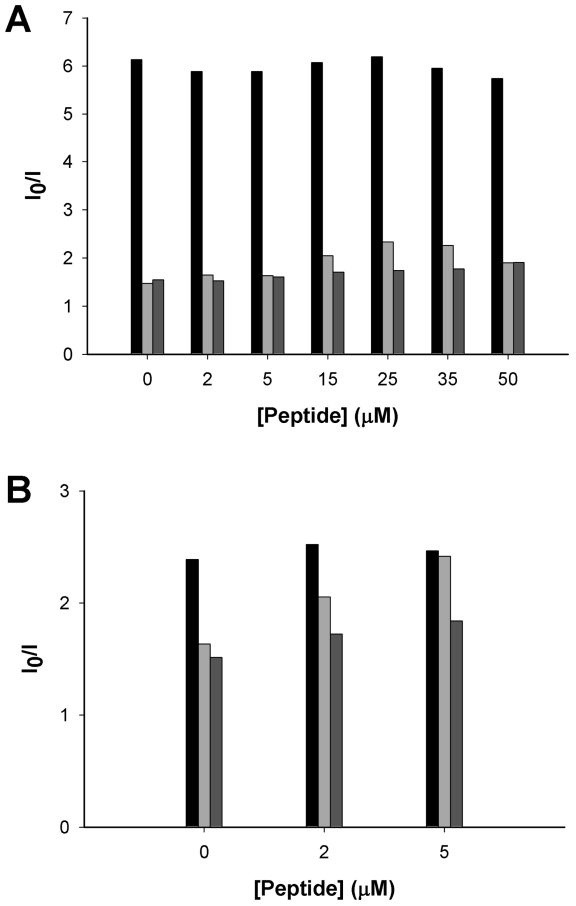

FIGURE 8: Evaluation of transbilayer channel formation induced by PrP(106−126)W (light gray) or PrP(106−126) (dark gray) in 100 μM POPC/POPG (1:1) vesicles (MLVs) followed by NBD quenching by Co^{2+}. The ratio of NBD fluorescence emission ($\lambda_{excitation}$ = 460 nm) in the absence of quencher (I_0) and in presence of 20 mM Co^{2+} (I) for the vesicles with Co^{2+} accessible to both layers (black columns) and for the vesicles where Co^{2+} is only accessible to the outer layer (gray columns) is presented for different peptide concentrations. These experiments were carried at pH 5 with 150 mM NaCl (A) or at pH 5 with 10 mM NaCl (B).

In the present work, the membrane binding mechanism of PrP(106−126) was further studied with a modified peptide, PrP(106−126)W. The tryptophan residue enhances the hydrophobicity (Figure 1) without perturbing the pI or amphipathicity of the peptide, with an increased propensity to interact with lipid bilayers expected based on White and Wimley analysis (*33*). The use of PrP (106−126)W therefore provides an opportunity to dissect the role of membrane interaction in neurotoxicity by increasing the peptide concentration at the membrane without significantly perturbing the physicochemical properties of the peptide. The present work was carried out with model membranes in different buffer conditions: pH 7.4 and 150 mM NaCl to model cytoplasmic physiological conditions; pH 5 and 150 mM NaCl to mimic the endosomal environment, and pH 5 and 10 mM NaCl to evaluate the contribution of electrostatic interaction to membrane affinity. In addition to fluorescence-based studies, peptide−lipid interactions were followed by SPR and structurally by circular dichroism.

The results show that PrP(106−126)W aggregates in an aqueous environment, with the aggregates having discrete hydrophobic pockets (Figures 2). At pH 7.4, a

heterogeneous population of aggregates was verified by DLS and by REES. At acidic pH, a reorganization seems to occur as revealed by tryptophan fluorescence emission properties (Figure 2B) and by an ANS fluorescence intensity decrease (Figure 2D) where a homogeneous population of aggregates seems to exist as verified by a monodisperse sample and by the lack of REES on peptide tryptophan fluorescence.

Fluorescence and SPR results clearly show that the insertion of a tryptophan residue significantly improves the membrane binding properties of PrP(106−126) in which its interaction with membrane is mainly governed by hydrophobic interaction (see Results section, Table 2 and Figure 4) due to tryptophan anchoring at the interfacial region (*43*). Once the peptide inserts into the membrane bilayer, a significant proportion of the bound peptide does not dissociate from the membrane (*29*−*31*,*43*). The binding is however enhanced in the presence of negatively charged phospholipids, at acidic pH and at low ionic strength (Table 1 and Figures 3, 4, and 6). Neither Chol nor GM1 increased the affinity of PrP(106−126)W for lipid membranes (see Table 2). Chol and gangliosides (e.g., GM1) are abundantly expressed in neuronal membranes and have been assumed to have a special role in neuronal cells (*44*). GM1 (*45*,*46*) and chol are concentrated in lipid raft regions, which have been implicated in prion disease (*47*,*48*). Our results further exclude a specific interaction of PrP(106−126) with any of these components in more rigid domains.

Previous reports have proposed that PrP(106−126) creates large nonselective ion channels and binds irreversibly (*13*,*14*). In a more recent study, semipenetrated poration was suggested by AFM observations, but the physiological meaning of such a semipenetrated pore is not clear (*15*). In the case of channel formation or semipenetrated poration induced by PrP(106−126), Co^{2+} ions should be able to access the NBD fluorophores on the inner layer and a quenching of NBD fluorescence emission would be expected. In the present work, while the modified PrP(106−126) with M112W substitution exhibits a much higher affinity for lipid bilayers even when physiological ionic strength is used, permeability to Co^{2+} was not detected. Leakage events were detected only with POPC/POPG (1:1) membranes at pH 5 and 10 mM NaCl (see Figure 8). Under these conditions, the number of peptide molecules inserted into the lipid bilayer is much higher than that observed for other conditions and is typical of membrane saturation (*35*,*49*). This suggests that membrane leakage only occurs when an excess of peptide concentration is in direct contact with the lipid matrix. Thus, for this particular peptide, an increase in affinity for lipid bilayers under physiological conditions did not correlate with an increase in membrane leakage (see Figure 8A).

In our previous study with PrP(106−126), we demonstrated a lack of pore formation together with an inability to interact with membranes at physiological conditions (*16*). We reasoned that increasing the ability to partition to membranes should subsequently increase the propensity for pore formation, and in the present work, it was verified that the affinity of PrP(106−126) for the membrane increases dramatically when a tryptophan residue is included in the sequence (see Figure 5). However, PrP(106−126)W did not form channels in either cytoplasmic or endosomal physiological conditions (see Figure 8A). This peptide therefore does not exhibit any propensity to significantly disturb the membrane even when designed to penetrate the membrane surface. Overall, these results provide further evidence against membrane pore formation playing any role in PrP(106−126) neurotoxicity and supports the proposal that PrP toxicity cannot be explained by the action of the PrP(106−126) fragment at the plasma membrane level.

REFERENCES

1. Prusiner, S. B. (1998) Prions. *Proc. Natl. Acad. Sci. U.S.A. 95*, 13363–83.
2. Stahl, N., Baldwin, M. A., Teplow, D. B., Hood, L., Gibson, B. W., Burlingame, A. L., and Prusiner, S. B. (1993) Structural studies of the scrapie prion protein using mass spectrometry and amino acid sequencing. *Biochemistry 32*, 1991–2002.
3. Prusiner, S. B. (1991) Molecular biology of prion diseases. *Science 252*, 1515–22.
4. Peters, P. J., Mironov, A.Jr., Peretz, D., van Donselaar, E., Leclerc, E., Erpel, S., DeArmond, S. J., Burton, D. R., Williamson, R. A., Vey, M., and Prusiner, S. B. (2003) Trafficking of prion proteins through a caveolae-mediated endosomal pathway. *J. Cell Biol. 162*, 703–17.
5. Fevrier, B., Vilette, D., Archer, F., Loew, D., Faigle, W., Vidal, M., Laude, H., and Raposo, G. (2004) Cells release prions in association with exosomes. *Proc. Natl. Acad. Sci. U.S.A. 101*, 9683–8.
6. Kazlauskaite, J., and Pinheiro, T. J. (2005) Aggregation and fibrillization of prions in lipid membranes. *Biochem. Soc. Symp.* 211–22.
7. Naslavsky, N., Stein, R., Yanai, A., Friedlander, G., and Taraboulos, A. (1997) Characterization of detergent-insoluble complexes containing the cellular prion protein and its scrapie isoform. *J. Biol. Chem. 272*, 6324–31.
8. Forloni, G., Angeretti, N., Chiesa, R., Monzani, E., Salmona, M., Bugiani, O., and Tagliavini, F. (1993) Neurotoxicity of a prion protein fragment. *Nature 362*, 543–6.
9. Florio, T., Thellung, S., Amico, C., Robello, M., Salmona, M., Bugiani, O., Tagliavini, F., Forloni, G., and Schettini, G. (1998) Prion protein fragment 106−126 induces apoptotic cell death and impairment of L-type voltage-sensitive calcium channel activity in the GH3 cell line. *J. Neurosci. Res. 54*, 341–52.
10. Jobling, M. F., Stewart, L. R., White, A. R., McLean, C., Friedhuber, A., Maher, F., Beyreuther, K., Masters, C. L., Barrow, C. J., Collins, S. J., and Cappai, R. (1999) The hydrophobic core sequence modulates the neurotoxic and secondary structure properties of the prion peptide 106−126. *J. Neurochem. 73*, 1557–65.
11. Fioriti, L., Quaglio, E., Massignan, T., Colombo, L., Stewart, R. S., Salmona, M., Harris, D. A., Forloni, G., and Chiesa, R. (2005) The neurotoxicity of prion protein (PrP) peptide 106−126 is independent of the expression level of PrP and is not mediated by abnormal PrP species. *Mol. Cell. Neurosci. 28*, 165–76.
12. Salmona, M., Forloni, G., Diomede, L., Algeri, M., De Gioia, L., Angeretti, N., Giaccone, G., Tagliavini, F., and Bugiani, O. (1997) A neurotoxic and gliotrophic fragment of the prion protein increases plasma membrane microviscosity. *Neurobiol. Dis. 4*, 47–57.
13. Kourie, J. I., and Culverson, A. (2000) Prion peptide fragment PrP [106−126] forms distinct cation channel types. *J. Neurosci. Res. 62*, 120–33.
14. Lin, M. C., Mirzabekov, T., and Kagan, B. L. (1997) Channel formation by a neurotoxic prion protein fragment. *J. Biol. Chem. 272*, 44–7.
15. Zhong, J., Zheng, W., Huang, L., Hong, Y., Wang, L., Qiu, Y., and Sha, Y. (2007) PrP106−126 amide causes the semi-penetrated poration in the supported lipid bilayers. *Biochim. Biophys. Acta 1768*, 1420–9.
16. Henriques, S. T., Pattenden, L. K., Aguilar, M. I., and Castanho, M. A. (2008) PrP(106−126) does not interact with membranes under physiological conditions. *Biophys. J. 95*, 1877–89.
17. Gasset, M., Baldwin, M. A., Lloyd, D. H., Gabriel, J. M., Holtzman, D. M., Cohen, F., Fletterick, R., and Prusiner, S. B. (1992) Predicted α-helical regions of the prion protein when synthesized as peptides form amyloid. *Proc. Natl. Acad. Sci. U.S.A. 89*, 10940–4.

18. Henriques, S. T., and Castanho, M. A. (2005) Environmental factors that enhance the action of the cell penetrating peptide pep-1 A spectroscopic study using lipidic vesicles. *Biochim. Biophys. Acta 1669*, 75–86.
19. Santos, N. C., and Castanho, M. A. (1996) Teaching light scattering spectroscopy: The dimension and shape of tobacco mosaic virus. *Biophys. J. 71*, 1641–50.
20. McParland, V. J., Kad, N. M., Kalverda, A. P., Brown, A., Kirwin-Jones, P., Hunter, M. G., Sunde, M., and Radford, S. E. (2000) Partially unfolded states of beta(2)-microglobulin and amyloid formation in vitro. *Biochemistry 39*, 8735–46.
21. Santos, N. C., Prieto, M., and Castanho, M. A. (2003) Quantifying molecular partition into model systems of biomembranes: an emphasis on optical spectroscopic methods. *Biochim. Biophys. Acta 1612*, 123–35.
22. Mozsolits, H., Lee, T. H., Clayton, A. H., Sawyer, W. H., and Aguilar, M. I. (2004) The membrane-binding properties of a class A amphipathic peptide. *Eur. Biophys. J. 33*, 98–108.
23. Cladera, J., and O'Shea, P. (1998) Intramembrane molecular dipoles affect the membrane insertion and folding of a model amphiphilic peptide. *Biophys. J. 74*, 2434–42.
24. Clarke, R. J. (2001) The dipole potential of phospholipid membranes and methods for its detection. *Adv. Colloid Interface Sci. 89*−*90*, 263–81.
25. Shapovalov, V. L., Kotova, E. A., Rokitskaya, T. I., and Antonenko, Y. N. (1999) Effect of gramicidin A on the dipole potential of phospholipid membranes. *Biophys. J. 77*, 299–305.
26. Henriques, S. T., and Castanho, M. A. (2004) Consequences of nonlytic membrane perturbation to the translocation of the cell penetrating peptide pep-1 in lipidic vesicles. *Biochemistry 43*, 9716–24.
27. Killian, J. A., and von Heijne, G. (2000) How proteins adapt to a membrane-water interface. *Trends Biochem. Sci. 25*, 429–34.
28. Seelig, J. (2004) Thermodynamics of lipid-peptide interactions. *Biochim. Biophys. Acta 1666*, 40–50.
29. Lee, T. H., Mozsolits, H., and Aguilar, M. I. (2001) Measurement of the affinity of melittin for zwitterionic and anionic membranes using immobilized lipid biosensors. *J. Pept. Res. 58*, 464–76.
30. Mozsolits, H., Unabia, S., Ahmad, A., Morton, C. J., Thomas, W. G., and Aguilar, M. I. (2002) Electrostatic and hydrophobic forces tether the proximal region of the angiotensin II receptor (AT1A) carboxyl terminus to anionic lipids. *Biochemistry 41*, 7830–40.
31. Mozsolits, H., Wirth, H. J., Werkmeister, J., and Aguilar, M. I. (2001) Analysis of antimicrobial peptide interactions with hybrid bilayer membrane systems using surface plasmon resonance. *Biochim. Biophys. Acta 1512*, 64–76.
32. Henriques, S. T., Pattenden, L. K., Aguilar, M. I., and Castanho, M. A. R. B. ((2008)) PrP(106−126) does not interact with membranes in physiological conditions. *Biophys. J.*, submitted for publication.
33. White, S. H., and Wimley, W. C. (1998) Hydrophobic interactions of peptides with membrane interfaces. *Biochim. Biophys. Acta 1376*, 339–52.
34. Veiga, A. S., Santos, N. C., Loura, L. M., Fedorov, A., and Castanho, M. A. (2004) HIV fusion inhibitor peptide T-1249 is able to insert or adsorb to lipidic bilayers. Putative correlation with improved efficiency. *J. Am. Chem. Soc. 126*, 14758–63.
35. Melo, M. N., and Castanho, M. A. (2007) Omiganan interaction with bacterial membranes and cell wall models. Assigning a biological role to saturation. *Biochim. Biophys. Acta 1768*, 1277–90.
36. Cox, D. L., Sing, R. R., and Yang, S. (2006) Prion disease: Exponential growth requires membrane binding. *Biophys. J. 90*, L77–9.
37. Thellung, S., Florio, T., Corsaro, A., Arena, S., Merlino, M., Salmona, M., Tagliavini, F., Bugiani, O., Forloni, G., and Schettini, G. (2000) Intracellular mechanisms mediating the neuronal death and astrogliosis induced by the prion protein fragment 106−126. *Int. J. Dev. Neurosci. 18*, 481–92.
38. Kourie, J. I. (2001) Mechanisms of prion-induced modifications in membrane transport properties: implications for signal transduction and neurotoxicity. *Chem. Biol. Interact. 138*, 1–26.
39. Miura, T., Yoda, M., Takaku, N., Hirose, T., and Takeuchi, H. (2007) Clustered negative charges on the lipid membrane surface induce beta-sheet formation of prion protein fragment 106−126. *Biochemistry 46*, 11589–97.
40. Dupiereux, I., Zorzi, W., Lins, L., Brasseur, R., Colson, P., Heinen, E., and Elmoualij, B. (2005) Interaction of the 106−126 prion peptide with lipid membranes and potential implication for neurotoxicity. *Biochem. Biophys. Res. Commun. 331*, 894–901.
41. Kunz, B., Sandmeier, E., and Christen, P. (1999) Neurotoxicity of prion peptide 106−126 not confirmed. *FEBS Lett. 458*, 65–8.
42. Manunta, M., Kunz, B., Sandmeier, E., Christen, P., and Schindler, H. (2000) Reported channel formation by prion protein fragment 106−126 in planar lipid bilayers cannot be reproduced. *FEBS Lett. 474*, 255–6.
43. Jin, Y., Mozsolits, H., Hammer, J., Zmuda, E., Zhu, F., Zhang, Y., Aguilar, M. I., and Blazyk, J. (2003) Influence of tryptophan on lipid binding of linear amphipathic cationic antimicrobial peptides. *Biochemistry 42*, 9395–405.
44. Norton, W. T., Abe, T., Poduslo, S. E., and DeVries, G. H. (1975) The lipid composition of isolated brain cells and axons. *J. Neurosci. Res. 1*, 57–75.
45. Kakio, A., Nishimoto, S., Yanagisawa, K., Kozutsumi, Y., and Matsuzaki, K. (2002) Interactions of amyloid beta-protein with various gangliosides in raft-like membranes: importance of GM1 ganglioside-bound form as an endogenous seed for Alzheimer amyloid. *Biochemistry 41*, 7385–90.
46. Matsuzaki, K., Noguch, T., Wakabayashi, M., Ikeda, K., Okada, T., Ohashi, Y., Hoshino, M., and Naiki, H. (2007) Inhibitors of amyloid beta-protein aggregation mediated by GM1-containing raft-like membranes. *Biochim. Biophys. Acta 1768*, 122–30.
47. Taylor, D. R., and Hooper, N. M. (2006) The prion protein and lipid rafts. *Mol. Membr. Biol. 23*, 89–99.
48. Sarnataro, D., Campana, V., Paladino, S., Stornaiuolo, M., Nitsch, L., and Zurzolo, C. (2004) PrP(C) association with lipid rafts in the early secretory pathway stabilizes its cellular conformation. *Mol. Biol. Cell 15*, 4031–42.
49. Melo, M. N., Ferre, R., and Castanho, M. A. (2009) Antimicrobial peptides: linking partition, activity and high membrane-bound concentrations. *Nat. Rev. Microbiol. 7*, 245–50.